Phase transformations, crystal and magnetic structures of high-pressure hydrides of *d*-metals

V.E. Antonov*

Institute of Solid State Physics, Russian Academy of Sciences, 142432 Chernogolovka, Moscow District, Russia

Abstract

This paper will briefly discuss the high-pressure-hydrogen techniques used at the Institute of Solid State Physics, Russian Academy of Sciences, the T–P diagrams of the studied binary metal–hydrogen systems and the crystal and magnetic structures of high-pressure hydrides formed in those systems. A compilation of the available experimental data and a list of relevant publications are provided for reference purposes. © 2002 Elsevier Science B.V. All rights reserved.

Keywords: Metal hydrides; Crystal structure; Magnetic properties

1. Introduction

Most transition metals form hydrides at sufficiently high pressures of hydrogen. The technique for compressing gaseous hydrogen to pressures of up to 9 GPa at temperatures up to 500°C [1], and recently to 1000°C [2], developed at the Institute of Solid State Physics, Russian Academy of Sciences (ISSP RAS), made it possible to synthesise hydrides of all 3*d*-metals and of all 4*d*-metals except Ru. In particular, hydrides of Fe, Co, Mo, Tc, Rh and Re have been synthesised at the ISSP for the first time.

The technique also allows the rapid cooling of the hydrides under high pressure to liquid nitrogen temperature. At such a low temperature all hydrides are metastable at ambient pressure and can be removed from the high-pressure cell for studying their composition, crystal structure and physical properties.

At the ISSP RAS, hydrogen is compressed in the capsules shown in Fig. 1, which are placed in a quasihydrostatic Toroid-type high-pressure chamber. Hydrogen gas inside the capsule is produced by thermal decomposition of AlH_3 after a preliminary compression. If a Teflon capsule is used, the dead space in it is initially filled with heptane or silicon oil to prevent leaks of hydrogen, which forms a bubble around the sample in the upper part of the capsule. To seal a copper capsule, the gap between the capsule and the plug is filled with gallium, which is liquid at ambient temperature, diffuses into the

copper when the temperature is raised and forms Cu–Ga alloys of increasing thermal stability as its concentration in the copper matrix decreases. Teflon, Cu and Ga are largely impermeable to hydrogen. The dead space in the copper capsule is filled with kaolin wool which does not react with H_2, Cu and *d*-metals in the T–P range of interest. Due to the hardness of its fibres, the wool remains porous even at high pressures, leaving enough room for the hydrogen gas inside the capsule and ensuring good access of the hydrogen to the sample. The maximum amount of hydride produced in one experiment varies from 30 to 500 mm^3 depending on the pressure of synthesis.

The high-pressure technique has been most effective in hydrogenation of the group VI–VIII transition metals, neither of which except Pd forms hydrides at low hydrogen pressures. The hydrides formed at high pressures were shown to have close-packed metal sublattices with *fcc* (γ), *hcp* (ϵ) or *double hcp* (ϵ') structures, in which hydrogen occupies octahedral interstitial positions. The hydrides are metals and most of them exist in wide composition ranges and can be considered as solid solutions of hydrogen distributed over interstices either randomly or in a superstructure order. According to the phase rule, only single-phase fields are possible in the equilibrium T–P diagrams of binary Me–H systems, but the composition of every phase can vary with T and P within the corresponding field. The T–P diagrams constructed at the ISSP RAS and also the diagram of the Pd–H system from literature [3] are presented in Fig. 2. The solid lines show the transitions accompanied by a decrease in the hydrogen content of the sample (hydride decomposition), as these lines are much

E-mail address: antonov@issp.ac.ru (V.E. Antonov).
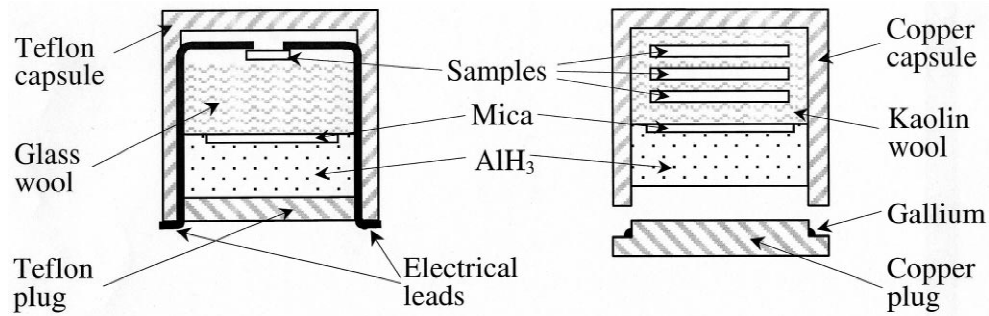
Fig. 1. Schematic diagrams of the high-pressure cells used for electrical measurements [1] (left) and for production of hydrides [2] (right).

closer to the equilibrium phase boundaries than the lines of hydride formation [4].

Table 1 compiles the neutron diffraction data of our group on the crystal and magnetic structure of Me–H phases prepared under a high hydrogen pressure and studied in a metastable state at ambient pressure and also literature data on ε-CrH and γ-PdH.

2. Formation conditions and structures of high-pressure hydrides

Cr–H system: The hydrogen solubility in *bcc* (α) chromium is small. Chromium hydride with a *hcp* (ε) metal lattice can be produced electrolytically and under high hydrogen pressure [5]. Its composition is always close to CrH. The NiAs-type (Fig. 3a) crystal structure of ε-CrH was determined by neutron diffraction using the sample loaded with hydrogen electrolytically [6] while the values of lattice parameters indicated in Table 1 were more accurately determined by X-ray diffraction on the sample synthesised under a high hydrogen pressure [5].

Mn–H system: At atmospheric pressure, there are four allotropic modifications of manganese: α-Mn and β-Mn with complex cubic lattices, *fcc* γ-Mn and *bcc* δ-Mn. Under high pressures of hydrogen, manganese forms ε hydrides [7,8] with the H-to-metal atomic ratio x ranging from 0.65 to 0.96 [9], γ hydrides with $0 < x < 0.5$ [10] and also primary solid solutions of hydrogen in α-Mn and β-Mn with $x \leq 0.1$ [2].

In the ε manganese hydrides with $x \geq 0.83$, hydrogen atoms are randomly distributed over octahedral interstices in the *hcp* metal lattice (a deficient NiAs type structure, Fig. 3a) [11]. At $x = 0.65$, hydrogen forms a superstructure, presumably, of the anti-CdI_2 type [12] shown in Fig. 3b. The hydrides are antiferromagnets with the Néel temperature of $T_N \approx 360$ K and have a layered collinear spin structure formed of ferromagnetic $(110)_{hex}$ planes coupled antiferromagnetically [11,12] as shown in Fig. 4a.

The γ hydride $MnH_{0.41}$ has a *fcc* metal lattice with $a_0 = 3.776$ Å at 300 K, in which hydrogen randomly occupies octahedral interstices [13]. The hydride is an antiferromagnet with $T_N >> 300$ K and a layered collinear structure formed of ferromagnetic (001) planes coupled antiferromagnetically [13] as shown in Fig. 4b. Its magnetic Bravais cell is tetragonal with $a = a_0/\sqrt{2}$ and $c = a_0$ (Table 1).

In α-$MnH_{0.073}$, hydrogen randomly occupies interstitial positions of the 12*e* type inside distorted octahedra of manganese atoms [14] as shown in Fig. 5. The 12*e* sites form dumb-bells 0.68 Å long positioned at the centres of the edges and faces of the cubic unit cell of α-Mn. Because of the small distance between the sites in a dumb-bell, these positions cannot be occupied by hydrogen at the same time due to the 'blocking effect' [15] requiring that the distance between hydrogen atoms in a metal should not be less than 2 Å. There are 58 manganese atoms in the unit cell of α-Mn, and occupancy of half of 12*e* sites corresponds to a H/Mn atomic ratio of $x = 6/58 \approx 0.103$. Thus, about 70% of the accessible interstices were filled with hydrogen in the α-$MnH_{0.073}$ solid solution studied.

The small distance of 0.68 Å between the sites in a dumb-bell also results in a giant effect of hydrogen tunnelling which is clearly visible in the inelastic neutron scattering spectra of α-$MnH_{0.073}$ even at temperatures as high as 100 K [14,16]. Using ^{119}Sn Mössbauer spectroscopy it was shown that T_N of α-Mn doped with 0.2 at.% Sn increases from 97 to 128 K on dissolution of $x = 0.05$ of hydrogen [17].

Fe–H system: The hydrogen solubility in α-Fe is small. Iron forms *dhcp* ε′ hydride with $x \approx 1$ [18,19], *fcc* γ hydride of unknown composition [20] and also a metastable intermediate *hcp* ε phase [20] with $x \approx 0.4$ [21].

The ε′ iron hydride is a ferromagnet with the Curie temperature much exceeding 300 K [22]. ^{57}Fe Mössbauer spectroscopy revealed a large concentration of stacking faults in its *dhcp* metal lattice [23]. In the neutron diffraction investigation [21], the stacking faults manifested themselves by the presence of Fe and H atoms on 'defect' 2*d* and 4*f* sites as indicated in the last two lines of description of ε′-FeH in Table 1. The schematic plot of the ε′-FeH crystal structure in Fig. 6 shows displacements of hydrogen layers that are not indicated in Table 1 because the effect was largely within the error limits. Nevertheless, these displacements of the order of $\delta Z = 0.007c \approx 0.03$ Å
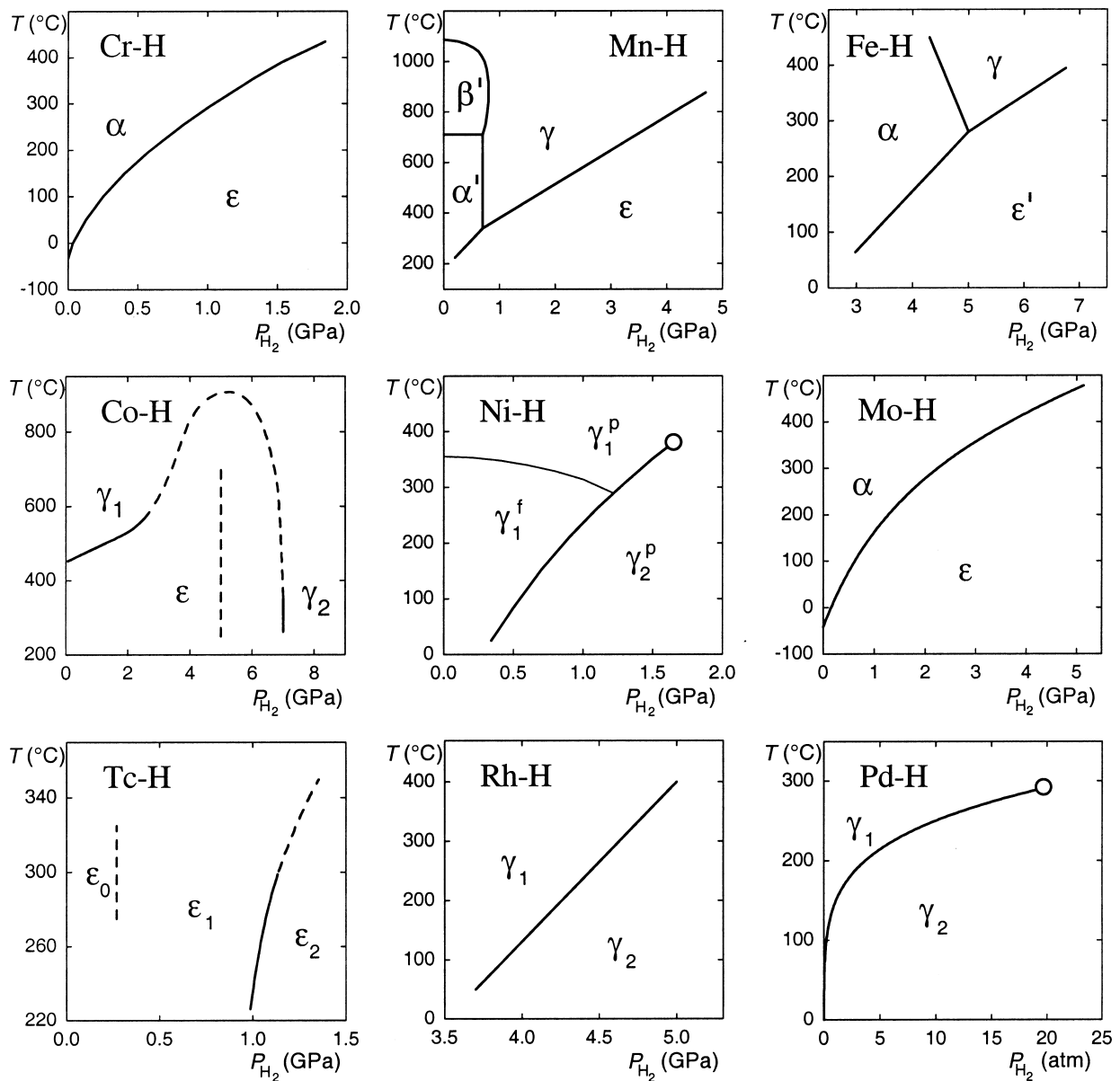
Fig. 2. *T–P* diagrams of the systems Cr–H [42], Mn–H [2], Fe–H [43], Co–H [24,44], Ni–H [28], Mo–H [45], Tc–H [32,33], Rh–H [37] and Pd–H [3]. Metal lattices of the phases are: α = *bcc*, α′ = α-Mn, β′ = β-Mn, γ = *fcc*, ε = *hcp*, ε′ = *dhcp*. The subscripts '0', '1' and '2' mark isomorphous phases in the order of increasing hydrogen content. The superscripts 'f' and 'p' mark ferro- and paramagnetic phases, respectively. The dashed portion of the ε→γ boundary in the Co–H diagram is tentative. The vertical dashed line in this diagram is a schematic plot of the line of supercritical anomalies of the transformation between the metastable γ_1 and γ_2 phases. The dashed curves in the Tc–H diagram represent the lines of supercritical anomalies of the $\epsilon_0 \leftrightarrow \epsilon_1$ and $\epsilon_1 \leftrightarrow \epsilon_2$ transformations. The circles in the Ni–H and Pd–H diagrams show the position of the critical point of the $\gamma_1 \leftrightarrow \gamma_2$ transformation (the γ_1 and γ_2 phase in the Pd–H system are usually called the α and β phase, respectively).

are very likely to occur on physical grounds [21] as they increase the distance between hydrogen atoms in equally stacked octahedral layers that is the shortest distance between any hydrogen atoms in the hydride. This is the very effect one can expect in view of the strong long-range repulsive interaction between hydrogen atoms, which is one of the main factors governing formation of hydrides of transition metals [15].

The ϵ-FeH$_{0.42}$ hydride is paramagnetic down to 4.2 K

[21,23]. Hydrogen is randomly distributed over octahedral interstices of the *hcp* metal lattice [21].

Co–H system: At temperatures of 250–350°C, the equilibrium solubility of hydrogen in the low-temperature *hcp* (ε) modification of cobalt monotonically increases with pressure and reaches $x \approx 0.6$ at 7 GPa [24]. At higher pressures, hydride with $x \approx 1$ is formed on the base of the high-temperature *fcc* (γ) cobalt modification [24]. A neutron diffraction investigation at ambient pressure and

Table 1
Positional parameters (X, Y, Z) and site occupancies for high-pressure hydrides of the group VI–VIII transition metals

Phase	Atom	Site	X	Y	Z	Occupancy	Ref.
ϵ-CrH$_x$; $x = 1.00$, $T = 300$ K; $P6_3/mmc$, $M = 2$	Cr	$2c$	1/3	2/3	1/4	1.00	[5,6]
$a = 2.717$ Å, $c = 4.436$ Å, $c/a = 1.633$	H	$2a$	0	0	0	1.00	
ϵ-MnH$_x$; $x = 0.83$, $T = 120$ K; $P6_3/mmc$, $M = 2$	Mn	$2c$	1/3	2/3	1/4	1.00	[11]
$a = 2.692$ Å, $c = 4.355$ Å, $c/a = 1.618$	H	$2a$	0	0	0	0.83	
AFM, $\sigma = 0.73$ μ_B/Mn atom							
γ-MnH$_x$; $x = 0.41$, $T = 300$ K; P_I4/mmm, $M = 2$	Mn, $\sigma\uparrow$	$1a$	0	0	0	1.00	[13]
$a = 2.670$ Å, $c = 3.776$ Å, $c/a = \sqrt{2}$	Mn, $\sigma\downarrow$	$1d$	1/2	1/2	1/2	1.00	
AFM, $\sigma = 1.88$ μ_B/Mn atom	H	$1b$	0	0	1/2	0.41	
	H	$1c$	1/2	1/2	0	0.41	
α-MnH$_x$; $x = 0.073$, $T = 300$ K;	Mn	$2a$	0	0	0	1.00	[14]
$I\bar{4}3/mmc$, $M = 58$	Mn	$8c$	0.319	0.319	0.319	1.00	
$a = 8.9403$ Å	Mn	$24g_1$	0.355	0.355	0.034	1.00	
	Mn	$24g_2$	0.091	0.091	0.281	1.00	
	H	$12e$	0	0	0.538	0.34	
ϵ'-FeH$_x$; $x = 1.00$, $T = 90$ K; $P6_3/mmc$, $M = 4$	Fe	$2a$	0	0	0	1.000	[21]
$a = 2.679$ Å, $c = 8.77$ Å, $c/a = 2 \cdot 1.637$	Fe	$2c$	1/3	2/3	1/4	0.935	
FM, $\sigma = 2.2$ μ_B/Fe atom	H	$4f$	1/3	2/3	7/8	0.935	
	Fe	$2d$	1/3	2/3	3/4	0.065	
	H	$4f$	1/3	2/3	1/8	0.065	
ϵ-FeD$_x$; $x = 0.42$, $T = 90$ K; $P6_3/mmc$, $M = 2$	Fe	$2c$	1/3	2/3	1/4	1.00	[21]
$a = 2.583$ Å, $c = 4.176$ Å, $c/a = 1.617$	D	$2a$	0	0	0	0.42	
ϵ-CoH$_x$; $x = 0.26$, $T = 120$ K; $P6_3/mmc$, $M = 2$	Co	$2c$	1/3	2/3	1/4	1.00	[25]
$a = 2.544$ Å, $c = 4.116$ Å, $c/a = 1.618$	H	$2a$	0	0	0	0.26	
FM, $\sigma = 1.6$ μ_B/Co atom							
ϵ-CoH$_x$; $x = 0.34$, $T = 120$ K; $P6_3$, $M = 6$	Co	$2b$	1/3	2/3	1/12	1.00	[25]
$a = 2.555$ Å, $c = 12.406$ Å, $c/a = 3 \cdot 1.619$	Co	$2b$	2/3	1/3	0.245	1.00	
FM, $\sigma = 1.6$ μ_B/Co atom	Co	$2b$	1/3	2/3	0.421	1.00	
	H	$2a$	0	0	1/6	0.02	
	H	$2a$	0	0	0	0.02	
	H	$2a$	0	0	1/3	0.97	
ϵ-CoD$_x$; $x = 0.50$, $T = 120$ K; $P\bar{3}m1$, $M = 2$	Co	$2d$	1/3	2/3	0.262	1.00	[25]
$a = 2.579$ Å, $c = 4.162$ Å, $c/a = 1.614$	D	$1a$	0	0	0	0.97	
FM, $\sigma = 1.5$ μ_B/Co atom	D	$1b$	0	0	1/2	0.04	
γ-NiH$_x$; $x = 1.05$, $T = 120$ K; $Fm3m$, $M = 4$	Ni	$4a$	0	0	0	1.00	[31]
$a = 3.740$ Å	H	$4b$	1/2	1/2	1/2	1.00	
ϵ-MoH$_x$; $x = 1.05$, $T = 120$ K; $P6_3/mmc$, $M = 2$	Mo	$2c$	1/3	2/3	1/4	1.00	[31]
$a = 2.937$ Å, $c = 4.758$ Å, $c/a = 1.620$	H	$2a$	0	0	0	0.95	
ϵ-TcH$_x$; $x = 0.45$, $T = 300$ K; $P\bar{3}m1$, $M = 2$	Tc	$2d$	1/3	2/3	0.26	1.00	[34]
$a = 2.801$ Å, $c = 4.454$ Å, $c/a = 1.590$	H	$1a$	0	0	0	0.90	
	H	$1b$	0	0	1/2	≈ 0	
ϵ-TcH$_x$; $x = 0.69$, $T = 300$ K; $P6_3/mmc$, $M = 2$	Tc	$2c$	1/3	2/3	1/4	1.00	[34]
$a = 2.838$ Å, $c = 4.465$ Å, $c/a = 1.573$	H	$2a$	0	0	0	0.69	
γ-RhH$_x$; $x = 1.00$, $T = 120$ K; $Fm3m$, $M = 4$	Rh	$4a$	0	0	0	1.00	[31]
$a = 4.010$ Å	H	$4b$	1/2	1/2	1/2	0.95	
γ-PdH$_x$; $x = 1.00$, $T = 77$ K; $Fm3m$, $M = 4$	Pd	$4a$	0	0	0	1.00	[38,39]
$a = 4.090$ Å	H	$4b$	1/2	1/2	1/2	1.00	
ϵ-ReH$_x$; $x = 0.20$, $T = 90$ K; $P6_3/mmc$, $M = 2$	Re	$2c$	1/3	2/3	1/4	1.00	[12]
$a = 2.801$ Å, $c = 4.465$ Å, $c/a = 1.594$	H	$2a$	0	0	0	0.20	

T is the temperature of the neutron diffraction measurement; M is the number of formula units per unit cell, σ is the magnetic moment.
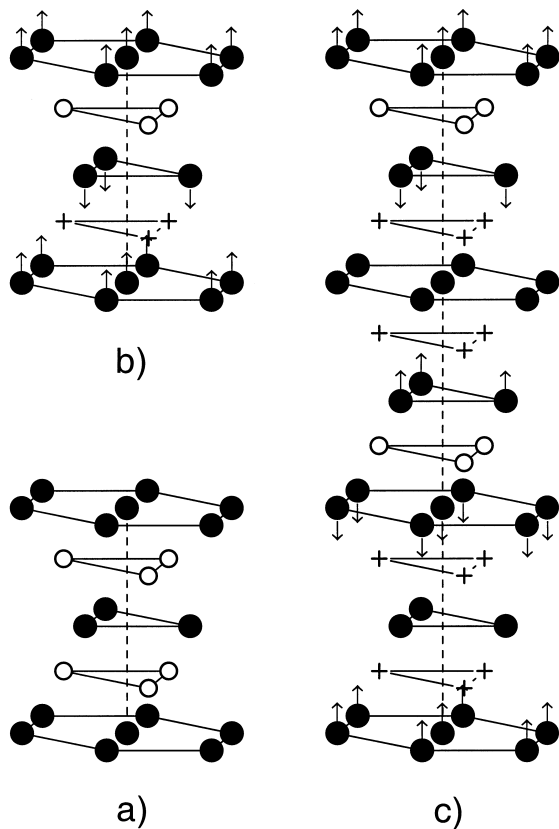
Fig. 3. Crystal structures of ϵ hydrides: (a) the NiAs type structure, space group $P6_3/mmc$; (b) the anti-CdI$_2$ type structure, $P\bar{3}m1$; (c) the Co$_3$H structure, $P6_3$. The solid circles show positions of metal atoms. The crosses and open circles mark octahedral interstitial positions, respectively, empty and occupied by hydrogen atoms. The arrows indicate the directions of displacements of metal atoms from the *hcp* positions due to hydrogen ordering.

Fig. 4. Crystal (solid lines) and magnetic (dashed lines) Bravais cells of manganese hydrides. (a) ϵ-MnH$_{0.83}$: a deficient NiAs type crystal structure, space group $P6_3/mmc$; an orthorhombic magnetic structure, Shubnikov space group P_Ccmm [11]. (b) γ-MnH$_{0.41}$: a deficient NaCl type crystal structure, $Fm3m$; a tetragonal magnetic structure, P_I4mmm [13]. Solid circles represent manganese atoms, open circles show the octahedral positions partly occupied by hydrogen, arrows indicate the positions and directions of the magnetic moments.

120 K showed [25] that hydrogen atoms in the ϵ solutions with $x \leq 0.26$ are randomly distributed over octahedral interstices (Fig. 3a). In the solutions with $x \geq 0.34$, hydrogen atoms form layered superstructures, occupying every third octahedral base layer at $x = 0.34$ (Fig. 3c) and every second layer at $x \geq 0.38$ (Fig. 3b). In the ordered structures, as seen from Table 1 and Fig. 3b and c, the metal layers separated by hydrogen atoms move apart while the layers containing nearly no hydrogen between them move closer together. Cobalt and its hydrides are ferromagnets. The magnetic moments in the ϵ hydrides are directed along the *c*-axis and decrease with increasing hydrogen concentration at a rate of about 0.36 Bohr magneton per H atom [26].

Ni–H system: Nickel hydride is formed via the isomorphous $\gamma_1 \rightarrow \gamma_2$ transition and can be produced electrolytically and under high hydrogen pressure [27]. At room temperature, the $\gamma_1 \rightarrow \gamma_2$ transition is accompanied by an abrupt increase in the hydrogen solubility from $x = 0.01$ to $x \approx 1$ [24]. The compositions of the coexisting γ_1 and γ_2 phases get closer to each other with increasing temperature, and the line of the $\gamma_1 \leftrightarrow \gamma_2$ equilibrium terminates at a

critical point [28] as shown in Fig. 2. The Curie temperature of the ferromagnetic γ_1 solutions decreases with hydrogen pressure due to the increase in the equilibrium

- Mn on 24g_1 - Mn on 24g_2 O - H on 12e
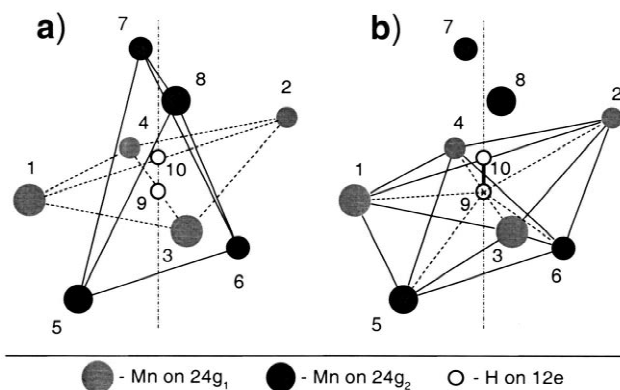
Fig. 5. A dumb-bell of two adjacent positions 12e partly occupied one at a time by hydrogen (open circles 9 and 10) and (a) its nearest neighbourhood of two tetrahedra formed by manganese atoms at positions 24g_1 (shaded circles 1–4) and at the positions 24g_2 (solid circles 5–8) and (b) the resulting distorted octahedral interstice around the 12e position (open circle 9) in the crystal structure of α-MnH$_{0.073}$ [14].
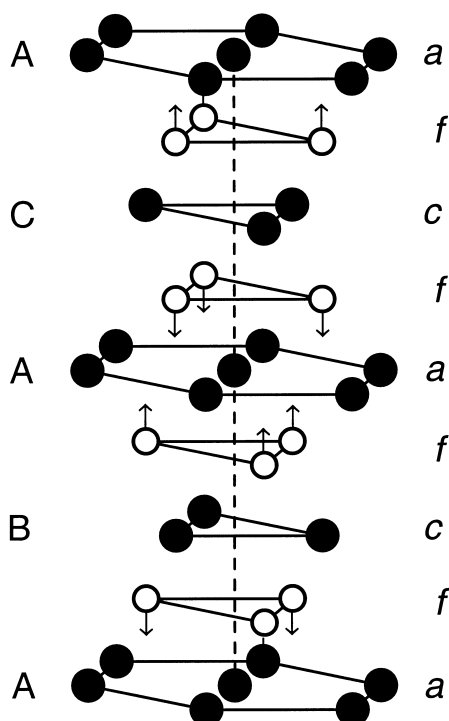
Fig. 6. Crystal structure of ϵ'-FeH [21]. The letters *a*, *c* and *f* mark the layers of equivalent positions in the $P6_3/mmc$ space group originated, respectively, from the positions 2*a*, 2*c* and 4*f* with Z=7/8 listed in Table 1. The solid circles show regular positions of Fe atoms, open circles of H atoms. The arrows indicate the directions of displacements of H atoms from the centres of octahedral interstices. The letters A, B and C represent the standard notation for close-packed layers in the *dhcp* structure.

hydrogen solubility [28]. The γ_2 phase is paramagnetic down to 4.2 K [29].

Mo–H system: The hydrogen solubility in *bcc* (α) molybdenum is small. The composition of the ϵ hydride is close to MoH [30,31].

Tc–H system: At high pressures, the system undergoes two isomorphous phase transitions, $\epsilon_0 \to \epsilon_1$ and $\epsilon_1 \to \epsilon_2$. The lines of both transitions terminate in the critical points at $T < 300°C$ [32,33]. At 300°C, the hydrogen solubility in Tc reaches $x \approx 0.5$ at 0.7 GPa and $x \approx 0.8$ at 2 GPa [33]. Under ambient conditions, hydrogen is randomly distributed over octahedral interstices in the hydride with $x = 0.69$ (a deficient NiAs type structure, Fig. 3a) and forms a layered superstructure of the anti-CdI$_2$ type (Fig. 3b) at $x = 0.45$ [34].

Ru–H system: The hydrogen solubility in *hcp* ruthenium at 250°C monotonically increases with pressure and reaches $x \approx 0.03$ at 9 GPa [35].

Rh–H system: The hydrogen content of the primary γ_1 solutions is small. The composition of the γ_2 hydride is close to RhH [36,37].

Pd–H system: A hydrogen pressure of about 0.007 atm is sufficient to form γ_2 hydride of palladium (usually called the β-phase) with $x \approx 0.61$ at room temperature [3], but pressures of the order of 1 GPa are necessary to approach $x = 1$ [38] (1 atm = 101 325 Pa). The octahedral hydrogen coordination in palladium hydrides was established by neutron diffraction for the sample with $x = 0.709$ [39]. The lattice parameter of γ-PdH indicated in Table 1 is from the X-ray measurements on the hydrides synthesised at high pressures [38].

Re–H system: At 170–300°C, the hydrogen solubility in *hcp* rhenium monotonically increases with pressure and reaches $x \approx 0.2$ at 9 GPa [40,41].

Concluding, it seems worth mentioning that the above variety of the magnetic properties and, to a great extent, of the crystal structures of high-pressure hydrides can be explained in the framework of a simple phenomenological 'rigid *d*-band' model [46].

Acknowledgements

References

[1] E.G. Ponyatovskii, V.E. Antonov, I.T. Belash, Sov. Phys. Usp. 25 (1982) 596.

[2] V.E. Antonov, T.E. Antonova, N.A. Chirin, E.G. Ponyatovsky, M. Baier, F.E. Wagner, Scripta Mater. 34 (1996) 1331.

[3] E. Wicke, H. Brodowsky, in: G. Alefeld, J. Völkl (Eds.), Hydrogen in Metals II, Springer, Berlin, 1978, p. 73.

[4] B. Baranowski, Ber. Bunsenges. Phys. Chem. 76 (1972) 714.

[5] B. Baranowski, K. Bojarski, Roczn. Chem. 46 (1962) 525.

[6] G. Albrecht, F.-D. Doenitz, K. Kleinstück, M. Betzl, Phys. Stat. Sol. 3 (1963) K249.

[7] M. Krukowski, B. Baranowski, Roczn. Chem. 49 (1975) 1183.

[8] E.G. Ponyatovskii, I.T. Belash, Dokl. Akad. Nauk SSSR 224 (1975) 607, in Russian.

[9] I.T. Belash, B.K. Ponomarev, V.G. Tissen, N.S. Afonokova, V.Sh. Shekhtman, E.G. Ponyatovskii, Fiz. Tverd. Tela (Leningrad) 20 (1978) 422, in Russian.

[10] Y. Fukai, H. Ishikawa, T. Goto, J. Susaki, T. Yagi, J.L. Soubeyrox, D. Fruchart, Z. Phys. Chem. N.F. 163 (1989) 479.

[11] A.V. Irodova, V.P. Glazkov, V.A. Somenkov, S.Sh. Shil'shtein, V.E. Antonov, E.G. Ponyatovskii, Sov. Phys. Solid State 29 (1987) 1562.

[12] S.Sh. Shilstein, V.P. Glazkov, A.V. Irodova, V.A. Somenkov, V.E. Antonov, E.G. Ponyatovskii, Z. Phys. Chem. N.F. 146 (1985) 129.

[13] V.K. Fedotov, V.E. Antonov, A.I. Kolesnikov, A.I. Beskrovnyi, G. Grosse, F.E. Wagner, Solid State Commun. 107 (1998) 787.

[14] V.K. Fedotov, V.E. Antonov, K. Cornell, G. Grosse, A.I. Kolesnikov, V.V. Sikolenko, V.V. Sumin, F.E. Wagner, H. Wipf, J. Phys.: Condens. Matter 10 (1998) 5255.

[15] V.A. Somenkov, V.P. Glazkov, Z. Phys. Chem. N.F. 117 (1979) 125.

[16] A.I. Kolesnikov, V.E. Antonov, S.M. Bennington, B. Dorner, V.K. Fedotov, G. Grosse, J.C. Li, S.F. Parker, F.E. Wagner, Physica B 263–264 (1999) 421.

[17] G. Grosse, F.E. Wagner, V.E. Antonov, T.E. Antonova, Hyperfine Interactions C 3 (1998) 221.

[18] V.E. Antonov, I.T. Belash, V.F. Degtyareva, E.G. Ponyatovskii, V.I. Shiryaev, Dokl. Akad. Nauk SSSR 252 (1980) 1384; [Engl. Trans. Sov. Phys. Dokl. 24 (1980) 490].

[19] V.E. Antonov, I.T. Belash, V.F. Degtyareva, D.N. Mogilyansky, B.K. Ponomarev, V.Sh. Shekhtman, Int. J. Hydrogen Energy 14 (1989) 371.

[20] M. Yamakata, T. Yagi, W. Utsumi, Y. Fukai, Proc. Jpn. Acad. 68B (1992) 172.

[21] V.E. Antonov, K. Cornell, V.K. Fedotov, A.I. Kolesnikov, E.G. Ponyatovsky, V.I. Shiryaev, H. Wipf, J. Alloys Comp. 264 (1998) 214.

[22] V.E. Antonov, I.T. Belash, E.G. Ponyatovskii, V.G. Thiessen, V.I. Shiryaev, Phys. Stat. Sol. (a) 65 (1981) K43.

[23] G. Schneider, M. Baier, R. Wordel, F.E. Wagner, V.E. Antonov, E.G. Ponyatovsky, Yu. Kopilovskii, E. Makarov, J. Less-Common Met. 172–174 (1991) 333.

[24] V.E. Antonov, I.T. Belash, V.Yu. Malyshev, E.G. Ponyatovskii, Dokl. Akad. Nauk SSSR 272 (1983) 1147, in Russian.

[25] V.K. Fedotov, V.E. Antonov, T.E. Antonova, E.L. Bokhenkov, B. Dorner, G. Grosse, F.E. Wagner, J. Alloys Comp. 291 (1999) 1.

[26] I.T. Belash, V.Yu. Malyshev, B.K. Ponomarev, E.G. Ponyatovskii, A.Yu. Sokolov, Sov. Phys. Solid State 28 (1986) 741.

[27] B. Baranowski, R. Wiśniewski, Bull. Acad. Polon. Sci. 14 (1966) 273.

[28] V.E. Antonov, I.T. Belash, E.G. Ponyatovskii, Dokl. Akad. Nauk SSSR 233 (1977) 1114, in Russian.

[29] V.G. Tissen, V.E. Antonov, I.T. Belash, B.K. Ponomarev, E.G. Ponyatovskii, Dokl. Akad. Nauk SSSR 242 (1978) 1390, in Russian.

[30] I.T. Belash, V.E. Antonov, E.G. Ponyatovskii, Dokl. Akad. Nauk SSSR 235 (1977) 379, in Russian.

[31] A.V. Irodova, V.P. Glazkov, V.A. Somenkov, S.Sh. Shil'shtein, V.E. Antonov, E.G. Ponyatovskii, Sov. Phys. Crystallogr. 33 (1988) 453.

[32] V.I. Spitsyn, E.G. Ponyatovskii, V.E. Antonov, I.T. Belash, O.A. Balakhovskii, Dokl. Akad. Nauk SSSR 247 (1979) 1420, in Russian.

[33] V.I. Spitsyn, V.E. Antonov, O.A. Balakhovskii, I.T. Belash, E.G. Ponyatovskii, V.I. Rashupkin, V.Sh. Shekhtman, Dokl. Akad. Nauk SSSR 260 (1981) 132, in Russian.

[34] V.P. Glazkov, A.V. Irodova, V.A. Somenkov, S.Sh. Shil'shtein, V.E. Antonov, E.G. Ponyatovskii, Sov. Phys. Solid State 26 (1984) 1961.

[35] V.E. Antonov, I.T. Belash, V.Yu. Malyshev, E.G. Ponyatovsky, Platinum Met. Rev. 28 (1984) 158; [Reprinted in: Int. J. Hydrogen Energy 11 (1986) 193].

[36] V.E. Antonov, I.T. Belash, V.F. Degtyareva, E.G. Ponyatovskii, Dokl. Akad. Nauk SSSR 239 (1978) 342, in Russian.

[37] V.E. Antonov, I.T. Belash, V.M. Koltygin, E.G. Ponyatovskii, Dokl. Akad. Nauk SSSR 248 (1979) 131, in Russian.

[38] J.E. Shirber, B. Morosin, Phys. Rev. B 12 (1975) 117.

[39] J.E. Worsham, M.K. Wilkinson, C.G. Shull, J. Phys. Chem. Solids 3 (1957) 303.

[40] V.E. Antonov, I.T. Belash, V.Yu. Malyshev, E.G. Ponyatovskii, N.A. Tulina, Dokl. Akad. Nauk SSSR 269 (1983) 617, in Russian.

[41] V.E. Antonov, I.T. Belash, O.V. Zharikov, A.V. Palnichenko, Phys. Stat. Sol. (b) 142 (1987) K155.

[42] E.G. Ponyatovskii, I.T. Belash, Dokl. Akad.Nauk SSSR 229 (1976) 1171, in Russian.

[43] V.E. Antonov, I.T. Belash, E.G. Ponyatovsky, Scripta Metal. 16 (1982) 203.

[44] V.E. Antonov, T.E. Antonova, M. Baier, G. Grosse, F.E. Wagner, J. Alloys Comp. 239 (1996) 198.

[45] V.E. Antonov, I.T. Belash, E.G. Ponyatovskii, Dokl. Akad. Nauk SSSR 248 (1979) 635, in Russian.

[46] V.E. Antonov, in: A. Gonis, P.E.A. Turchi, J. Kudrnovsky (Eds.), Stability of Materials, Plenum Press, New York, 1996, p. 725.